Modelling analysis of the influence of shield crossing on deformation and force in a large diaphragm wall

Guojun Wu[a,*], Shanpo Jia[b,*], Weizhong Chen[a,c], Jianping Yang[a], Jingqiang Yuan[a]

[a] *State Key Laboratory of Geomechanics and Geotechnical Engineering, Institute of Rock and Soil Mechanics, Chinese Academy of Sciences, Wuhan 430071, China*
[b] *Research Center of Geomechanics and Geotechnical Engineering, Yangtze University, Jingzhou 434023, Hubei, China*
[c] *Research Center of Geotechnical&Structural Engineering, Shandong University, Jinan 250061, China*

A R T I C L E I N F O

A B S T R A C T

The effect of a shield crossing an existing underground infrastructure needs to be evaluated, yet there are few studies on this subject. In this study, to model the influence of a shield crossing on a large diaphragm wall, a detailed three-dimensional numerical model with special methods considering the effects of the panel joints and the shield crossing has been developed. The panel joints have been simulated by a HINGE mode of the connection type, and the effect of shield crossing has been realized by modelling the excavated concrete using the solid elements, which interact with the surrounding soils that have been simulated with the ground springs. After analysing the characteristics of the deformation, maximum and minimum principal stresses, vertical and circumferential bending moments in the diaphragm wall, the maximum deformation, and the largest maximum and minimum principal stresses are at the perimeter of the shield tunnel. Further, for the bending moment, the largest negative vertical and circumferential bending moments are at the perimeter of the shield tunnel, yet the largest positive vertical and circumferential bending moments are distributed around the perimeter of the shield tunnel. For the largest tensile stress and vertical bending moment, there are large changes in the diaphragm wall around the shield tunnel, which is detrimental to the diaphragm wall. Considering the effect of the shield crossing, the diaphragm wall should be reinforced according to the results of the numerical analysis during the design and construction stages.

1. Introduction

As a type of retaining structures, when a circular diaphragm wall is subjected to water and earth pressures, it can carry heavy loads, and circumferential and vertical bending moments due to its spatial arching effects (Bruce et al., 1992; Chen et al., 2012; Tan, 2015; Tan and Wang, 2015). Therefore, it is increasingly used as part of underground infrastructures. The circular diaphragm wall is commonly composed of separate wall panels and vertical joints between the wall panels. Using the vertical joints to connect these panels together, these separate panels are formed as a continuous monolithic structure (Emam, 1999).

As the panel joints (especially the vertical joints) are the weakest parts of a diaphragm wall, due to their function in connecting the panels, their role in influencing the load transfer mechanism of the panels is significant. Although many studies were performed on the installation of diaphragm walls and the construction of ground excavation in the theoretical and technological aspects (Comodromos et al., 2013; Demoor, 1994; Gourvenec and Powrie, 1999; Ng et al., 1995; Powrie and Li, 1991; Schafer and Triantafyllidis, 2004; Segura-Castillo et al.,

2014), there are only a few studies on the behaviours and performance of the joint system. Chen et al. (2016a, 2016b) investigated the effect of three main design parameters of longitudinal steel plates in cross-plate joints on the shear capacity with experimental results. Further, using three-dimensional finite-element modelling, they predicted the shear bearing behaviour of the cross-plate joints. After showing the possible damage failures of joints, Ewald and Schneider (2015) suggested that firm, straight, and clean joint must be implemented before concreting the secondary element in order to minimize the risk of diaphragm wall pits.

In recent years, there is an increase in the construction of vertical shafts and large-scale circular underground facilities, down to a depth of 60–100 m (Ariizumi et al., 1999; Goto et al., 1995). When a shield crosses shafts or diaphragm walls, due to the interaction of the shafts (walls) and the shield tunnel, large deformations and stresses in the shafts (walls) can occur, which threatens the safety and stability of the shafts (walls). Therefore, the effect of the shield crossing on the safety and stability of the shafts (walls) need to be evaluated (Wu et al., 2017). Using numerical modelling, similar studies have been carried out on the

---

influence of the shield crossing on the objects, such as buildings, tunnels, pile foundations and other structures (Liu et al., 2009; Sirivachiraporn and Phienwej, 2012; Wei, 2012; Xu et al., 2015; Yamaguchi et al., 1998). However, there are few studies on the influence of shield crossing on shafts or walls, including the distributions of the displacement, force (stress and moment) when the shield is shielding-in and shielding-out from the shafts (walls), which is a major concern for the stability of shafts (walls).

As discussed above, the shielding crossing and the way the load is transferred are the most important factors which impact the safety and stability of the retaining structures. In this study, a special modelling method has been developed to model a diaphragm wall being crossed through by a shield tunnel. The model can consider the influences of the shielding crossing through the diaphragm wall and the load transfer of the panel joints. Hence, it can be used to study the characteristics of the deformation and force (stress and moment) in the diaphragm wall influenced by the shield crossing. By establishing a three-dimensional numerical model, the influence of the shield crossing on the deformation and force (stress and moment) of a large diaphragm wall have been analysed and evaluated.

2. General situation of the diaphragm wall

The diaphragm wall, as a part of the Meizizhou ventilating shaft in Nanjing, China, is located in a pool at the tail of the Meizizhou isle. The Meizizhou ventilating shaft has been designed as a circular concrete structure, with a circular diaphragm wall, a lining wall and four reinforced concrete ring beams, as shown in Fig. 1. The four ring beams are the top ring beam, the first ring beam, the second ring beam and the third ring beam, and they are all used as purlins. The circular diaphragm wall has an inner diameter of 26.8 m, and an outer diameter of 29.2 m (i.e., the thickness is 1.2 m). Considering the foundation stability of the whole structure, the diaphragm wall will be constructed to the depth at the altitude of −54.452 m. Since the altitude of the ground level is +8 m, the length of the diaphragm wall is actually 62.452 m. The soils within the diaphragm wall have been excavated to the altitude of −36.452 m, where the base plate is built for sealing the whole ventilating shaft. After the diaphragm wall is completed, it will be crossed by a tunnel boring machine (TBM) to form a section of a shield tunnel for transportation. The diameter of the shield tunnel is 14.5 m,
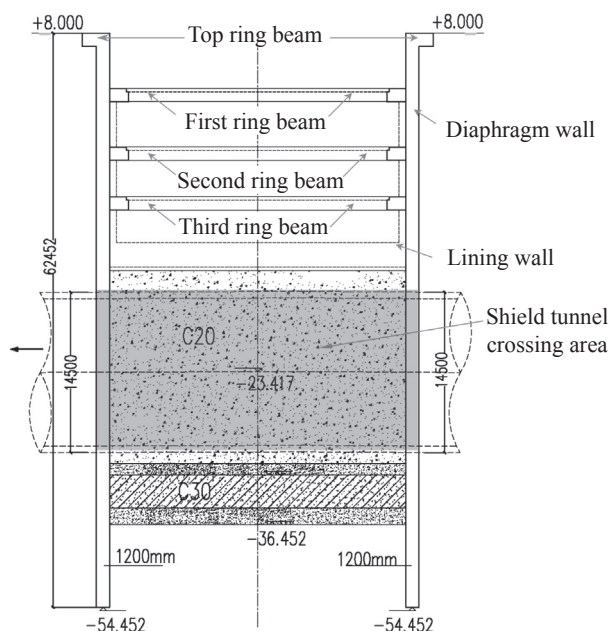
and the centre of the shield tunnel is positioned at the altitude of −23.417 m. From the top to the bottom of the diaphragm wall, the ground layers are silt, silty clay, fine sand, medium and coarse sand, respectively, whereas the bearing bed is in the pebble layer. In addition, the ventilating shaft is situated near an existing large levee, which has been used for flood prevention from the Yangtze River. Hence, the ventilating shaft is subjected to abundant water supply. Therefore, the engineering geology and hydrogeology conditions are challenging.

Being a challenging project, the Meizizhou ventilating shaft must meet the requirements of safety and stability during the construction, especially during the period when the shield tunnel crosses the diaphragm wall. Hence, it is regarded as a key part of the entire project. In this study, the numerical model has been used to analyse the Meizizhou ventilating shaft, and to determine the characteristics of the deformation and stress at the diaphragm wall. The results can then be used in the design and construction of the diaphragm wall.

3. Modelling of shield crossing the diaphragm wall with special methods

In order to study the stability and safety of the diaphragm wall when the shield crosses the ventilating shaft, numerical simulation is a desirable approach.

3.1. Numerical model

3.1.1. Model of the diaphragm wall

When establishing an analysis model for a diaphragm wall, the strata-structure model is often used to analyse the ground deformation and the interaction of the ground and the support structure (Jarddine et al., 1986). Further, if the emphasis is on the structure of the diaphragm wall, the load-structure model is often used to analyse the force/stress and the deformation in the diaphragm wall. In this study, the focus has been on the diaphragm wall considering the shield crossing. The ground outside the diaphragm wall can be ignored and the interaction of the ground and the structure can be simplified by using spring elements to link the ground to the structure, as shown in Fig. 4. In this way, the numerical simulation is less time-consuming. The numerical model has been developed using the code ABAQUS.

In this model, the diaphragm wall has 24 panels (Fig. 2), and the cross-plate joints (Wu et al., 2017) and the lining wall as well as the base plate of the lining are simulated using the three-dimensional shell elements. The ring beams (including the top ring beam) are simulated using the three-dimensional beam elements. In addition, the soil within the diaphragm wall, which will be excavated during the shield crossing, is simulated using the three-dimensional solid elements which interact with the diaphragm wall. These components of the ventilating shaft are shown in Fig. 3. For the modelling of the panel joints, and the crossing of the diaphragm wall by the shield, the details are in Sections 3.2 and
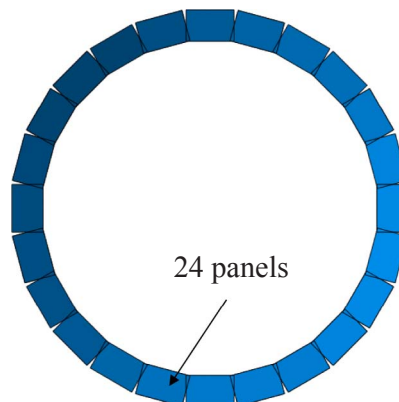

Fig. 1. Profile sketch of the Meizizhou ventilating shaft.

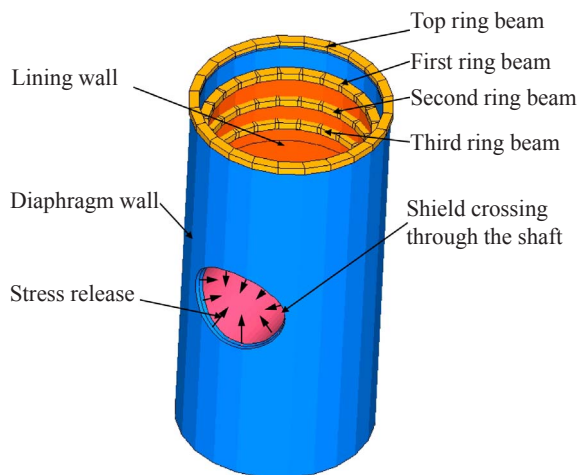**Fig. 2.** Plan view of the diaphragm wall with 24 panels.

Fig. 3. Diagram of the ventilating shaft.

3.3, respectively. There are 56,272 elements and 38,369 nodes in the model.

3.1.2. Boundary conditions

Except the external surfaces of the diaphragm wall which are restrained by the normal ground springs, the bottom edge of the diaphragm wall is fixed in the vertical direction, and the active earth pressure and external water pressure are applied to the surface of the diaphragm wall (Fig. 4). In addition, due to the existence of the base plate (which is located at the altitude of −36.452 m, as shown in Fig. 1), the uplift water pressure corresponding to its depth is applied to the outer surface of the base plate, as shown in Fig. 4. The unit elastic resistance coefficient of the ground springs is set at 1.7×10^7 N/m.

3.1.3. Model parameters

In this model, the diaphragm wall and the lining wall as well as the four ring beams are modelled as a type of reinforced concrete material. Due to the replacement of the excavated soil with plain concrete, which is used for shield crossing, the plain concrete within the shield crossing is modelled as C20 plain concrete, and the base plate below the excavated concrete is modelled as C30 plain concrete. The model parameters of the reinforced concrete and the plain concrete are shown in Table 1.

Fig. 4. Schematic diagram of the ventilating shaft with boundary conditions.

Table 1
Parameters used to model reinforced concrete and plain concrete.

Material	Unit weight ρ (kN/m³)	Elastic modulus E (GPa)	Poisson's ratio μ
Reinforced concrete	25	30	0.2
C20 plain concrete	24	25.5	0.2
C30 plain concrete	24	30	0.2

3.2. Modelling method for shield crossing the diaphragm wall

To ensure the safety of a shield crossing, the soils within the shield tunnel has to be excavated during the ventilating shaft construction and replace them with plain concrete so as to maintain its mechanical homogeneity. This is a good preparation for the shield crossing at the demand of the shielding. In this study, a special modelling method has been developed to achieve the effect of excavation when the shield crosses the diaphragm wall as follows. The plain concrete, which will be excavated during the shield crossing, is simulated with the three dimensional solid elements. Further, as the concrete interacts with the corresponding areas of the diaphragm wall; both lateral sides of the excavated concrete (including the shielding-in and shielding-out areas) are restrained with ground springs, as illustrated in Fig. 5. These ground springs are considered as a type of resistance springs, which can only carry compressive forces and not tensile forces.

To model the shield crossing through the diaphragm wall (including the shielding-in and shielding-out areas), in addition to the excavated plain concrete elements, the ground springs at both sides of the excavated concrete corresponding to the shielding-in and shielding-out areas are all removed, thereby realizing the effects of the stress release and deformation development of the diaphragm wall, as illustrated in Fig. 3. This modelling method does not only provide an equivalent model of the shield crosses the diaphragm wall, but provides a less expensive model without simulating the surrounding soil.

3.3. Modelling method for panel joints

The diaphragm wall consists of panels as well as joints between the panels, as shown in Fig. 6. Although it is known that the joints between the panels can significantly affect the stability of the diaphragm walls, there are few studies on the effect of the model panel joint stiffness on the deformation and stress of circular diaphragm walls. In this study, the HINGE mode of the connection types in ABAQUS has been used to model the panel joints in the diaphragm wall. In this way, the model is close to the practical situation.

3.3.1. Modelling panel joints outside the zone of shield crossing

The joints outside the zone of shield crossing are modelled with the connection type element HINGE in ABAQUS. The element HINGE has been used to join the positions of two nodes (i.e., nodes a and b, as shown in Fig. 7) and to provide a revolute constraint between their rotational degrees of freedom. The connection type HINGE imposes kinematic constraints and uses local orientation definitions. The predefined Coulomb-like friction in the HINGE connection relates the kinematic constraint forces and moments in the connector to a friction moment in the rotation about the HINGE axis. A typical interpretation of the geometric scaling constants is illustrated in Fig. 8.

As the rotation about the 1-direction is the only possible relative motion in the connection, the frictional effect is formally written in terms of the moments generated by the tangential tractions and the moments generated by the contact forces, as follows:

$$\varphi = P(f) - \mu M_N \leqslant 0 \tag{1}$$

where φ is the frictional effect, the potential $P(f)$ is the moment of the frictional tangential tractions in the connector in the direction

ground springs
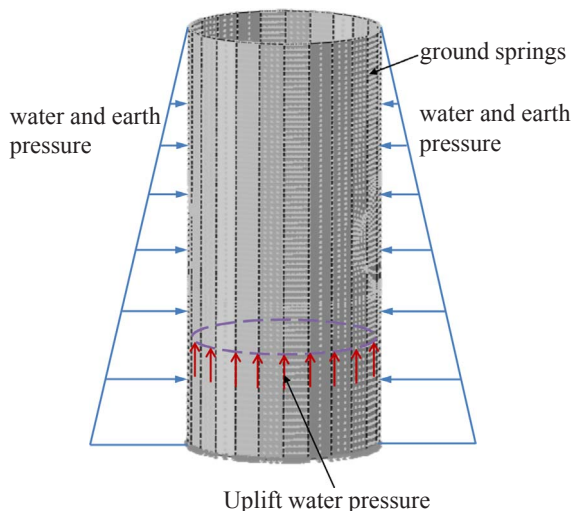
shielding-out area

Shield crossing block

shielding-in area
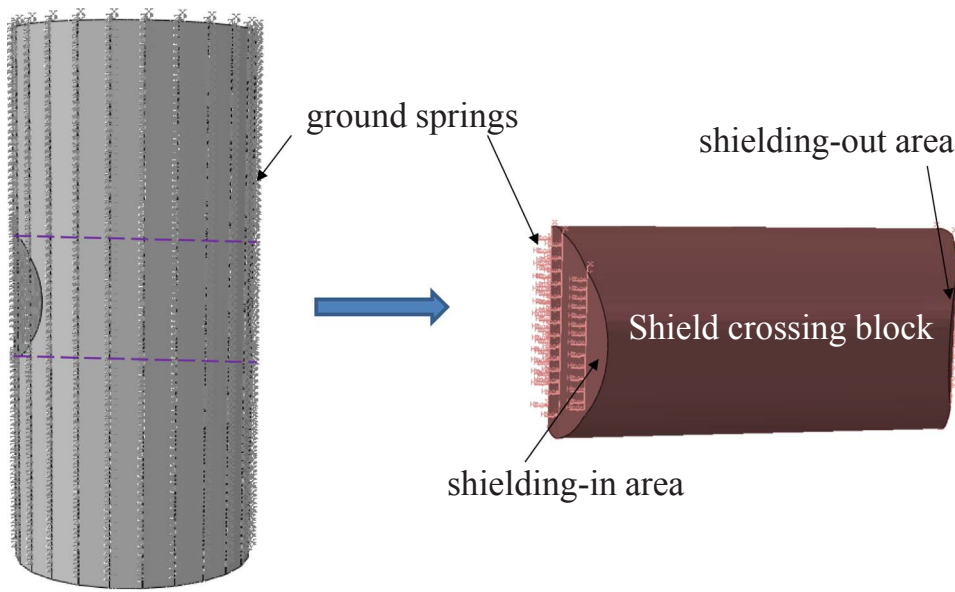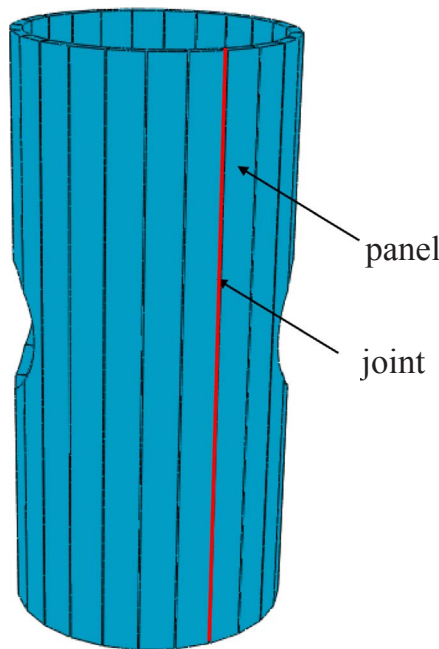
Fig. 6. Modelling joints between panels of a diaphragm wall.
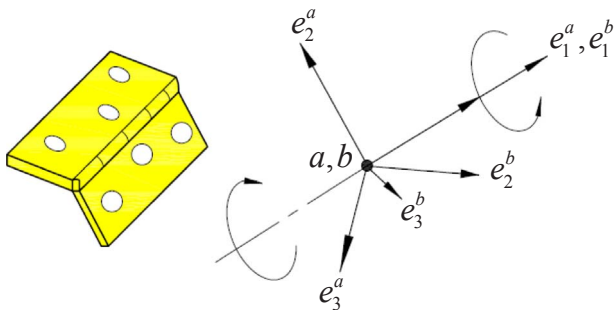
panel

joint

Fig. 7. The connection type HINGE and a local cylindrical coordinate system.

tangential to the cylindrical surface on which the contact occurs, M_N is the friction-producing normal moment on the same cylindrical surface, and μ is the friction coefficient. Frictional stick occurs if $\varphi < 0$. Sliding

Fig. 8. Illustration of the geometry for a HINGE connection.

occurs if $\varphi = 0$, and the friction moment is μM_N.

The normal moment, M_N, is the sum of the friction-producing connector moment, $M_C = g(f)$, and a self-equilibrated internal contact moment (such as from a press-fit assembly), M_C^{int}:

$$M_N = |M_C + M_C^{int}| = |g(f) + M_C^{int}| \tag{2}$$

M_C can be expressed as

$$M_C = g(f) = F_a R_a + F_n R_p \tag{3}$$

where $F_a R_a$ is the moment from the axial force, $F_a = |f_1|$ (i.e., an effective friction in the axial direction), and R_a is the effective friction arm associated with the constraint force in the axial direction; $F_n R_p$ is the moment from the forces normal to the cylindrical face, R_p is the radius of the pin cross-section in the local 2–3 plane, and F_n is the normal force, which is the sum of the radial force contribution and the force contribution from bending, as follows:

$$F_n = F_r + F_{bend} \tag{4}$$

where $F_r = \sqrt{f_2^2 + f_3^2}$, and f_2, f_3 are the radial forces in the 2-direction
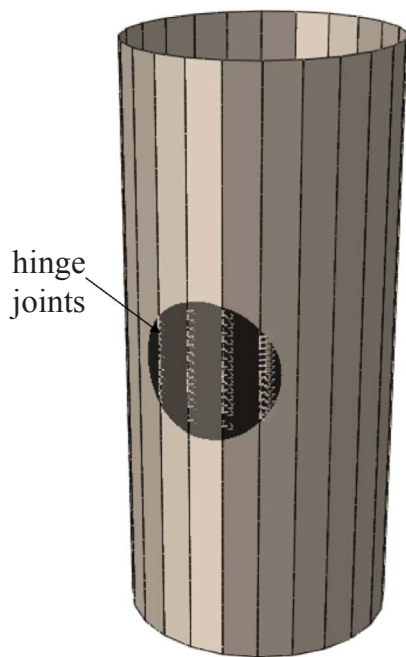
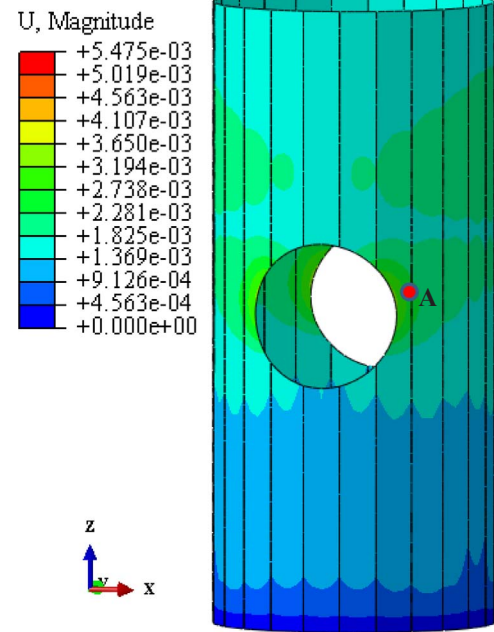**Fig. 9.** HINGE joints within the shield crossing zone.

Fig. 10. Deformation contour after shield crossing for Case 1.

and 3-direction, respectively; $F_{bend} = 2\frac{\sqrt{m_2^2 + m_3^2}}{L_s}$, and m_2, m_3 are the radial moments in the 2-direction and 3-direction, respectively, and L_s is the characteristic overlapping length between the pin and the sleeve (Fig. 8). In modelling the joints between panels, L_s has been set to zero. So, F_{bend} can be ignored.

In this modelling, it is required to define a local cylindrical coordinate system and to establish a connector behaviour and a connector section for each HINGE element. Once the elasticity stiffness of the connector is given, the deformation and stress distribution of the panels of the diaphragm walls can be derived through the numerical simulation. For the Meizizhou ventilating shaft, the connector elasticity stiffness has been set to 2×10^8 N/m.

3.3.2. Processing method of panel joints within the shield crossing zone

For the joints within the shield crossing zone, the modelling elements HINGE are active before the shield crossing. When the shield tunnel crosses, the elements HIINGE become deactive by setting up the keywords "model change, remove" in ABAQUS so as to eliminate these elements and to prevent them from being involved in the improvement of the computational efficiency. The HINGE elements that are eliminated with the soils within the shield crossing zone are shown in Fig. 9.

4. Analysis of the calculation results

For the diaphragm wall, the major concerns are the deformations and loads (i.e. stresses and moments) of the diaphragm wall influenced by the shield crossing, which are related to the stability and the practical design of the diaphragm wall.

4.1. Deformation of the diaphragm wall

Fig. 10 shows the deformation contour of the diaphragm wall after the shield tunnel has completely crossed. Due to the shield crosses the diaphragm wall, the plain concrete, as the excavated material, has been removed; and the deformations of the diaphragm wall, especially at the areas around and along the shield tunnel have been released. The maximum deformation, which is up to 5.44 mm, can be seen on the lateral sides of the shield tunnel, i.e. Point A near the shield tunnel as shown in Fig. 10, which is mainly characterized by the horizontal

deflection. Due to the symmetry of the model and boundary conditions, angle Φ has been defined anticlockwise from the top of the shield tunnel, and half of the tunnel perimeter with Φ = 0–180°, as shown in Fig. 11. From the deformation distribution along the perimeter, the maximum deformation (about 3.40 mm) along the perimeter is distributed at the location around 75° from the vault (Fig. 12), which indicates that the upper zones (where Φ < 90°) deforms larger than the lower zones (where Φ > 90°).

It is worth noting that the maximum deformation occurs at the time of shielding-in, when the zone will be used for shielding-out (i.e. the zone has not been removed yet) shows large deformation. Fig. 13 shows the deformation curves in the depth direction from the top of the diaphragm wall before and after the shield crossing. Due to the shield crossing, in the zone within the shield tunnel, there is a large change in the deformation, and the maximum deformation is 5.52 mm, which is
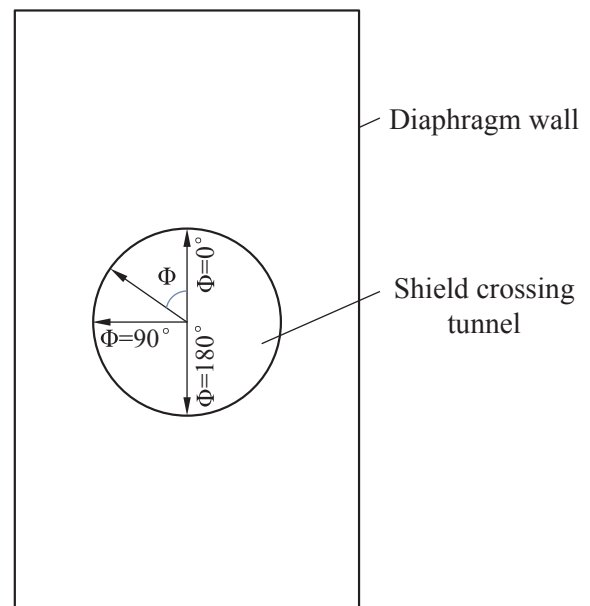

Fig. 11. Φ increases anticlockwise from the vault along the perimeter of the shield tunnel.
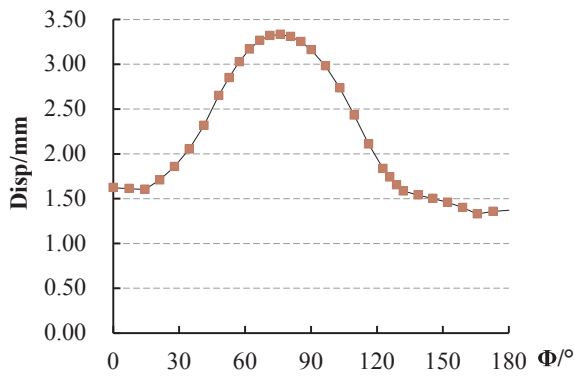
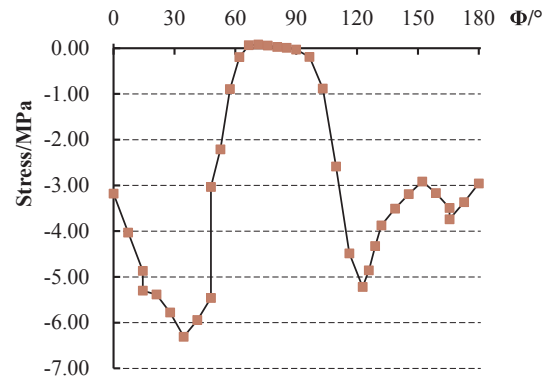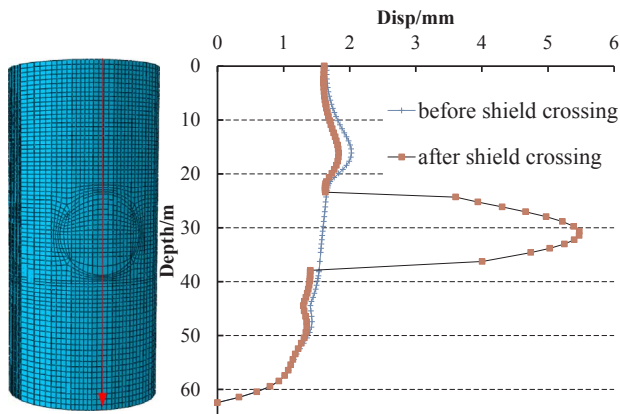Fig. 12. Deformation distribution along the perimeter of shield tunnel.

Fig. 13. Deformation curves along the depth direction from the top of the diaphragm wall.

located at the depth around 30 m from the top of the diaphragm wall. As a comparison, the deformation in the depth direction before the shield crossing is also shown. The deformation gradually decreases to zero at the bottom of the diaphragm wall. This is an indication that the shield crossing has a significant effect on the deformation of the diaphragm wall, especially at the zone around the shield tunnel.

4.2. Stress in the diaphragm wall

Due to the stress release induced by the shield crossing, there are large changes in the stresses in the diaphragm, especially at the perimeter of the shield tunnel. Fig. 14 shows the maximum principal stress distribution along the perimeter of the shield tunnel after the shield crossing. The positive maximum principal stresses are around 60–120°,
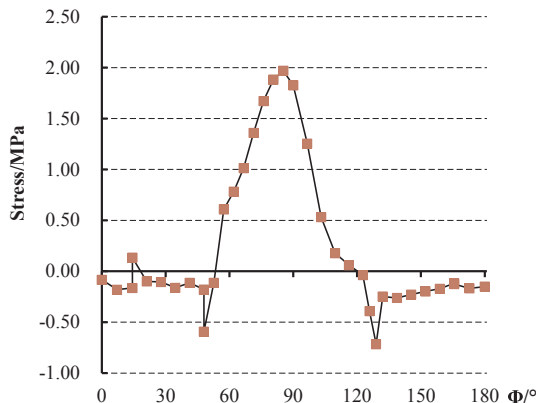

Fig. 14. Maximum principal stress distribution along the perimeter of shield tunnel.

Fig. 15. Minimum principal stress distribution along the perimeter of shield tunnel.

Table 2
Maximum and minimum principal stresses in the diaphragm wall.

	Maximum principal stress (MPa)	Minimum principal stress (MPa)
Before shield crossing	0.39	2.47
After shield crossing	1.99	6.32
Increment	410.26%	155.87%

and the largest stress is 1.99 MPa, which is located around 90°. This means that the relatively large positive (tensile) stresses are distributed at both lateral sides of the shield tunnel. Fig. 15 shows the minimum principal stress distribution along the perimeter of the shield tunnel after the shield crossing. The maximum and minimum principal stresses (according to the magnitudes) are mostly located at around 30° and 120°. This means that they are distributed at the upper and lower zones of both lateral sides of the shield tunnel.

Table 2 summaries the maximum and minimum principal stress in the diaphragm wall before and after the shield crossing. Comparing to the stresses before the shield crossing, the stresses after the shield crossing have increased by 410.26% and 155.87% for the maximum and minimum principal stresses, respectively. This shows that the shield crossing causes large changes to the stresses in the diaphragm wall, especially for the tensile stress around the shield tunnel, which is detrimental to the diaphragm wall.

4.3. Bending moment in the diaphragm wall

In the design of a diaphragm wall regarding its geometric shape, structure and the situation with the shield crossing, the bending moment is one of the major concerns which relates to the stability of the diaphragm wall. For a circular diaphragm wall, the vertical and circumferential bending moments should be of concern as they are the controlling factors.

In this study, the positive and negative bending moments refer to the directions opposite to each other, which follow the right-hand rule. For the vertical bending moment, the relative large positive bending moment are distributed 1.8 m above the shield tunnel. Fig. 16 shows the angle θ increases along the perimeter of the diaphragm wall at 1.8 m from the vault of the shield tunnel. Further, Fig. 17 shows the moment distribution curve along the perimeter of the diaphragm wall with θ = 0° to 180°. Since the model is symmetrical, this is why θ = 0–180° is chosen, and the sign of the moment is shown at lower right of Fig. 17. The curves are symmetrical about θ = 90°, and the maximal positive vertical bending moments are located around θ = 70° and θ = 110°, indicating that the maximal positive vertical bending moments are distributed at the upper right and upper left zones of the shield tunnel. However, the maximal negative vertical bending moment (i.e. 600 kN m as shown in Fig. 18) is at the perimeter of the shield
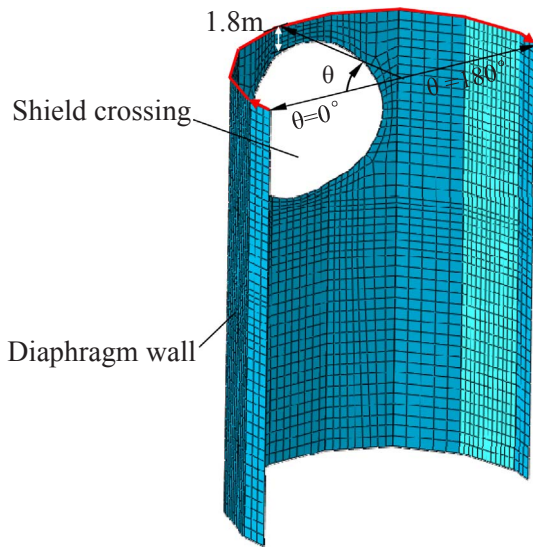
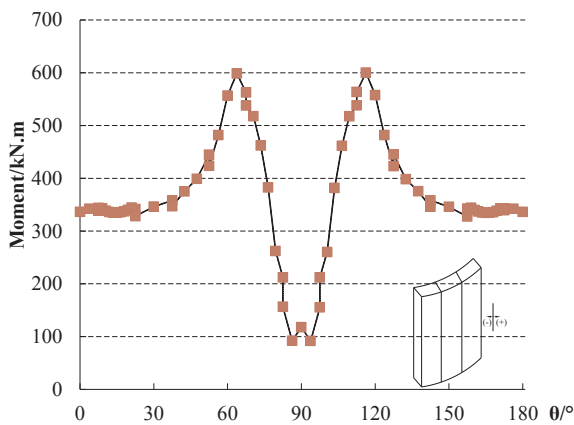**Fig. 16.** θ increases along the perimeter of the diaphragm wall at 1.8 m from the vault of shield tunnel.

Fig. 19. Circumferential bending moment in the diaphragm wall along the depth direction 1.9 m from the side of the shield tunnel.

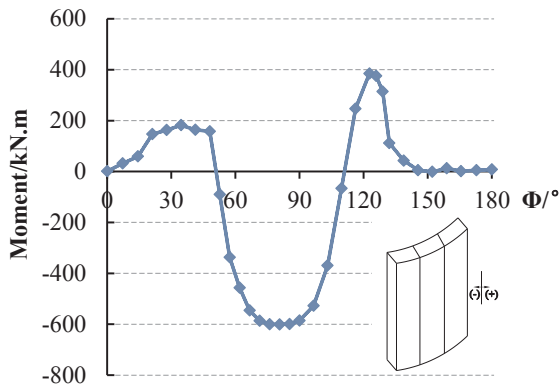**Fig. 17.** Vertical bending moment distribution along the perimeter of diaphragm wall.

Fig. 20. Circumferential bending moment distribution along the perimeter of shield tunnel.

Fig. 18. Vertical bending moment distribution along the perimeter of shield tunnel.

Table 3
Maximal vertical and circumferential bending moments in the diaphragm wall.

	Vertical bending moment (kN m)		Circumferential bending moment (kN m)	
	Positive	Negative	Positive	Negative
Before shield crossing	247	278	69.5	344
After shield crossing	811	600	126	557
Increment	228.34%	115.83%	81.29%	61.92%

tunnel at around Φ = 75° with the increase of angle Φ shown in Fig. 11, which indicates that the maximal negative vertical bending moment is located at the upper centre of the perimeter of the shield tunnel.

For the circumferential bending moment, the relative large positive bending moments are distributed at 1.9 m from the lateral sides of the shield tunnel. Fig. 19 shows the circumferential bending moments in the diaphragm wall in the depth direction via the 1.9 m point from the lateral sides of the shield tunnel. The maximal positive bending moment (i.e. 126 kN m) is located at the place with the depth = 30 m. However,
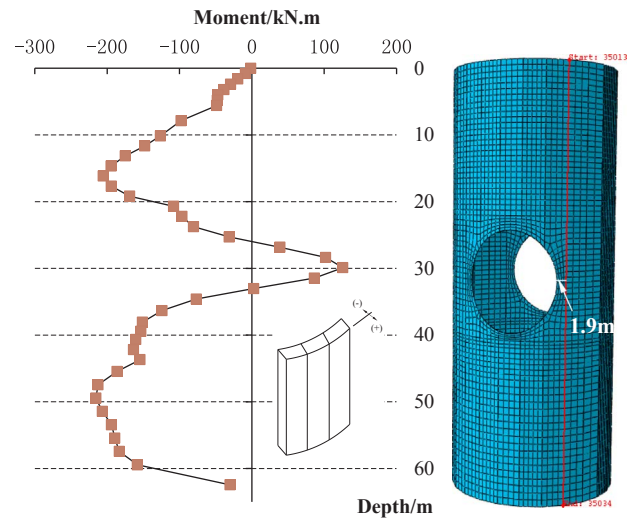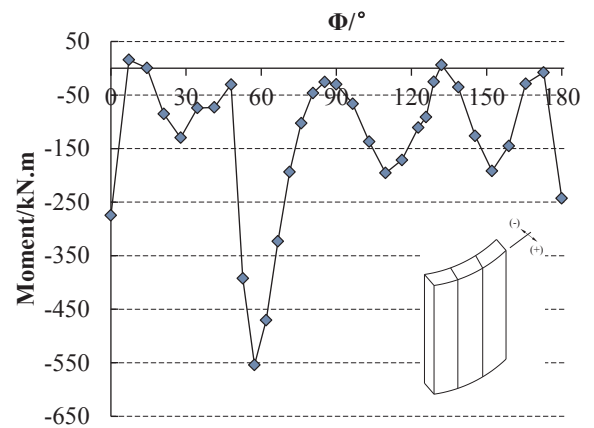
the maximal negative circumferential bending moment (i.e. 557 kN m) is at the perimeter of the shield tunnel, and at around Φ = 55° with the increase of angle Φ shown in Fig. 20, which indicates that the maximal negative circumferential bending moment is also located at the upper centre of the perimeter.

As a comparison, Table 3 summaries the maximal bending moments in the diaphragm wall before and after the shield crossing. For the vertical bending moments, comparing to the bending moments before the shield crossing, the bending moments after the shield crossing have increased by 228.34% and 115.83% for the maximal positive and negative vertical bending moments, respectively. For the circumferential bending moments, comparing to the bending moments before the shield

crossing, the bending moments after the shield crossing have increased by 81.29% and 61.92% for the maximal positive and negative circumferential bending moments, respectively. The results indicate that the shield crossing causes large changes in the bending moments in the diaphragm wall, especially for the change in the vertical bending moments around the shield tunnel, which is detrimental to the diaphragm wall.

4.4. Summary

Deformation: after the shield crosses the diaphragm wall, the maximum deformation (i.e. 5.52 mm) is near the lateral sides of the shield tunnel, which is much larger than that before the shield crossing.

Principal stress: after the shield crosses the diaphragm wall, the positive maximum principal stresses are mostly ranged from 60° to 120°, and the largest stresses are distributed at both lateral sides of the shield tunnel. Further, the maximal minimum principal stresses are mostly located at around 30° and 120°, distributed at the upper and lower zones of both lateral sides of the shield tunnel. In addition, the largest maximum and minimum principal stresses are increased by 410.26% and 155.87% comparing to those before the shield crossing.

Bending moment: for the vertical bending moments, the maximal positive bending moment is distributed at the upper zones of the shield tunnel, and the maximal negative bending moment is at the perimeter of the shield tunnel. For the circumferential bending moments, the maximal positive bending moment is distributed 1.9 m from the lateral sides of the shield tunnel, and the maximal negative bending moment is also at the perimeter of the shield tunnel. Accordingly, the influence of the shield crossing causes large changes in the bending moments in the diaphragm wall, especially for the change of the vertical bending moments around the shield tunnel.

In summary, the impact of the shield crossing on the deformation and force (stress and moment) in the diaphragm wall is large, which is detrimental to the diaphragm wall.

5. Conclusions

To obtain the exact characteristics of the deformation and force in the diaphragm wall, a detailed three-dimensional numerical model, with special methods considering the effects of panel joints and shield crossing, has been developed. The panel joints have been simulated by a HINGE mode of the connection type, and the effect of the shield crossing has been realized by modelling the excavated concrete using the solid elements, which interact with the surrounding soils that have been simulated with the ground springs.

According to the analysis of the deformation, principal stress and bending moment in the diaphragm wall, large changes have taken place due to the effect of shield crossing. The maximum deformation, and the largest maximum and minimum principal stresses are at the perimeter of the shield tunnel. Further, for the bending moment, the largest negative vertical and circumferential bending moments are at the perimeter of the shield tunnel, yet the largest positive vertical and circumferential bending moments are distributed around the perimeter of the shield tunnel. For the largest tensile stress and vertical bending moment, there are large changes in the diaphragm wall around the shield tunnel, which is detrimental to the diaphragm wall. Hence, it is concluded that the shield crossing has a significant effect on the deformation, stress and bending moment in the diaphragm wall.

Acknowledgements

The authors gratefully acknowledge the support of the National Natural Science Foundation of China (Grant Nos. 51379007, 41130742,

51678066), the support of the Chinese Fundamental Research (973) Program through the Grant No. 2013CB036006 and the support of the Youth Innovation Promotion Association, CAS.

Appendix A. Supplementary material

Supplementary data associated with this article can be found, in the online version, at http://dx.doi.org/10.1016/j.tust.2017.11.028.

References

Ariizumi, K., Kumagai, T., Kashiwagi, A., 1999. Behavior of large-scale cylindrical earth retaining wall, international Symposium on Geotechnical Aspects of Underground Construction in Soft Ground (IS-Tokyo 99). Geotechnical Aspects of Underground Construction in Soft Ground, Tokyo, Japan, pp. 481–486.
Bruce, D.A., Chan, P.H.C., Tamaro, G.J., 1992. Design, construction and performance of a deep circular diaphragm wall. In: Symposium on Slurry Walls: Design, Construction, and Quality Control. ASTM Special Technical Publication. American Society for Testing and Materials Special Technical Publication, Atlantic City, NJ, pp. 391–402.
Chen, F., Yang, G., Zhang, Y., Yao, L., 2012. Discussion on value of coefficient in structural design of circular diaphragm wall. Chin. J. Geotech. Eng. 34 (Suppl.), 203–206.
Chen, J., Hou, Y., Wang, J., Qiao, P., 2016a. Shear bearing of cross-plate joints between diaphragm wall panels – II: numerical analysis and prediction formula. Mag. Concrete Res. 68 (20), 1025–1039.
Chen, J.J., Wang, J.H., Qiao, P.Z., Hou, Y.M., Gu, Q.Y., 2016b. Shear bearing of cross-plate joints between diaphragm wall panels – I: model tests and shear behaviour. Mag. Concrete Res. 68 (17), 902–915.
Comodromos, E.M., Papadopoulou, M.C., Konstantinidis, G.K., 2013. Effects from diaphragm wall installation to surrounding soil and adjacent buildings. Comput. Geotech. 53, 106–121.
Demoor, E.K., 1994. An analysis of bored pile diaphragm wall installation effects. Geotechnique 44 (2), 341–347.
Emam, M., 1999. New method for construction of diaphragm walls. J. Constr. Eng. Manage.-ASCE 125 (4), 233–241.
Ewald, K., Schneider, N., 2015. Avoid of damage to diaphragm wall joints through the use of appropriate quality assurance systems. Bautechnik 92 (9), 631–637.
Goto, S., et al., 1995. Ground movement, earth and water pressures due to shaft excavations. In: International Symposium on Underground Construction in Soft Ground, New Delhi, India, pp. 151–154.
Gourvenec, S.M., Powrie, W., 1999. Three-dimensional finite-element analysis of diaphragm wall installation. Geotechnique 49 (6), 801–823.
Jarddine, R.J., Potts, D.M., Fourie, A.B., Burland, J.B., 1986. Studies of the influence of nonlinear stress-strain characteristics in soil structure interaction. Geotechnique 36 (3), 377–396.
Liu, H.Y., Small, J.C., Carter, J.P., Williams, D.J., 2009. Effects of tunnelling on existing support systems of perpendicularly crossing tunnels. Comput. Geotech. 36 (5), 880–894.
Ng, C., Lings, M.L., Simpson, B., Nash, D., 1995. An approximate analysis of the three-dimensional effects of diaphragm wall installation. Geotechnique 45 (3), 497–507.
Powrie, W., Li, E., 1991. Finite-element analysis of an insitu wall propped at formation level. Geotechnique 41 (4), 499–514.
Schafer, R., Triantafyllidis, T., 2004. Modelling of earth and water pressure development during diaphragm wall construction in soft clay. Int. J. Numer. Anal. Methods Geomech. 28 (13), 1305–1326.
Segura-Castillo, L., Josa, A., Aguado, A., 2014. Bi-layer diaphragm walls: parametric study of construction processes. Eng. Struct. 59, 608–618.
Sirivachiraporn, A., Phienwej, N., 2012. Ground movements in EPB shield tunneling of Bangkok subway project and impacts on adjacent buildings. Tunn. Undergr. Sp. Tech. 30, 10–24.
Tan, Y., 2015. Structural behaviors of large underground earth-retaining systems in shanghai. I: unpropped circular diaphragm wall. J. Perform. Constr. Fac. 29 (2), 04014058.
Tan, Y., Wang, D.L., 2015. Structural behaviors of large underground earth-retaining systems in Shanghai. II: multipropped rectangular diaphragm wall. J. Perform. Constr. Fac. 29 (2), 04014059.
Wei, G., 2012. Numerical simulation of shield tunnel crossing masonry structure building with various degrees. In: 4th International Conference on Technology of Architecture and Structure. Advanced Materials Research, Xian, pp. 889–893.
Wu, G.J., Chen, W.Z., Bian, H.B., Yuan, J.Q., 2017. Structure optimisation of a diaphragm wall with special modelling methods in a large-scale circular ventilating shaft considering shield crossing. Tunn. Undergr. Sp. Tech. 65, 35–41.
Xu, Q.W., et al., 2015. A case history of shield tunnel crossing through group pile foundation of a road bridge with pile underpinning technologies in Shanghai. Tunn. Undergr. Sp. Tech. 45, 20–33.
Yamaguchi, I., Yamazaki, I., Kiritani, Y., 1998. Study of ground-tunnel interactions of four shield tunnels driven in close proximity, in relation to design and construction of parallel shield tunnels. Tunn. Undergr. Sp. Tech. 13 (3), 289–304.